Advancements in lithium-ion battery recycling technologies: Exploring module-scale crushing and air separation techniques

Junhyun Choi [1], Kyeonghyeon Lee [1,2], Kwanho Kim [1,2], Hoon Lee [1,2]

[1] The Resources Utilization Division, Korea Institute of Geoscience and Mineral Resources (KIGAM), 124 Gwahak-ro, Yuseong-gu, Daejeon 34132, Republic of Korea

[2] Resource Engineering, University of Science and Technology, 124 Gwahak-ro, Yuseong-gu, Daejeon 34132, Republic of Korea

Corresponding authors: khkim@kigam.re.kr (Kwanho Kim), hoonlee@kigam.re.kr (Hoon Lee)

Abstract: The rapid expansion of electric vehicles (EVs) and renewable energy storage systems has driven a surge in the demand for lithium-ion batteries (LIBs), creating an urgent need for efficient and sustainable recycling technologies. As LIBs reach their end-of-life, the recovery of key materials, such as electrodes, separators, cell pouches, and plastics, is critical for both environmental protection and resource conservation. This study presents a novel zig-zag air separation technique, integrated with module-scale crushing, to optimize the recycling of crushed LIB modules. By fine-tuning particle size and airflow rates, the method effectively separates components larger than 2 mm, achieving recovery rates exceeding 95% for electrodes and cell pouches, and over 97% for plastics larger than 3.35 mm. The variability in plastic recovery highlights the necessity of precise particle size control. This approach not only enhances recycling efficiency but also reduces contamination risks and minimizes the burden on downstream processing steps. The findings demonstrate the potential of this technique as a scalable and sustainable solution to address the challenges of LIB recycling, offering a pathway to greater material circularity and reduced environmental impact.

Keywords: end-of-life battery, module, crushing, air classification, separation

1. Introduction

Lithium-ion batteries (LIBs) are critical to modern energy systems, providing high energy density, long cycle life, and scalability. These attributes have made them indispensable in electric vehicles (EVs), portable electronics, and renewable energy storage systems. With the rapid global adoption of EVs, the amount of LIB waste is expected to surpass 8 million tons annually by 2040. This surge in waste presents significant environmental and resource management challenges, underscoring the urgency for sustainable and efficient recycling solutions (Dunn et al., 2012; Wang et al., 2014; Fan et al., 2020). Recycling LIBs is crucial not only to mitigate environmental impacts but also to address the scarcity of critical raw materials such as lithium, cobalt, and nickel.

Spent LIBs are inherently complex, comprising a heterogeneous mix of materials. Each battery includes cathodes, anodes, separators, electrolytes, current collectors, and casing materials. Cathodes, composed of lithium nickel cobalt manganese oxide (NCM) or lithium iron phosphate (LFP), exhibit diverse chemical and physical properties, while the anodes primarily consist of graphite (Gaines, 2014; Zhang et al., 2018). Separators are made of polymeric materials like polyethylene or polypropylene, while current collectors utilize aluminum and copper (Georgi-Mascher et al., 2012). The outer casing, often steel or aluminum, and the volatile organic electrolytes further complicate recycling processes (Heelan et al., 2016). Effectively liberating and fractionating these components is essential to ensure high recovery rates and process efficiency (Li et al., 2010; Chen et al., 2019).

Mechanical pretreatment is the critical initial stage in LIB recycling, preparing batteries for subsequent recovery processes. Common mechanical techniques include shredding, crushing, sieving, and air classification, which are widely employed in both laboratory and industrial settings (Heelan et

al., 2016; Pinegar and Smith, 2019; Yan et al., 2023). Shredding and crushing effectively reduce battery size and liberate internal components. However, these methods often produce mixed fractions and fine particles, leading to contamination risks that hinder downstream recovery efficiency (Gratz et al., 2014; Velazquez-Martinez et al., 2019). For example, commingled active materials, plastics, and metal foils require additional separation steps, increasing complexity and costs (Chen et al., 2019). Sieving, while beneficial for size-based separation, struggles with overlapping size distributions, particularly in fine electrode particles and separator fragments (He et al., 2023; Makuza et al., 2021). Air classification, which relies on density differences to segregate materials, is promising but faces challenges when separating components like plastics and aluminum casings, whose densities are similar, leading to reduced recovery efficiency (Chen et al., 2019; Yan et al., 2023). Recent advancements in mechanical pretreatment and material recovery processes, such as density-based separation and optimized flotation techniques, have shown potential for high recovery rates of critical components in specific contexts (He et al., 2023; Wagner-Wenz et al., 2023). Hydrometallurgical recycling methods, although well-established, present challenges such as high energy consumption and environmental impact due to chemical usage. Changes and Pospiech (2013) highlighted hydrometallurgical technologies' potential to selectively recover valuable metals, but these methods require effective pretreatment to optimize material separation efficiency.

These shortcomings highlight the need for advanced pretreatment methods that can enhance separation efficiency while minimizing material losses (Yan et al., 2023). Furthermore, existing LIB recycling practices often depend on cell-level disassembly, which is labor-intensive and exposes operators to safety risks like thermal runaway during the crushing process (Velazquez-Martinez et al., 2019; Heelan et al., 2016). These challenges are further compounded by the non-standardized designs of LIBs, frequent use of adhesives, and variability in battery chemistries (Gaines, 2014; Xu et al., 2008; Changes and Pospiech, 2013). While module-level recycling offers potential to address these inefficiencies by enabling simultaneous processing of larger batches, it remains an underexplored avenue despite its scalability and cost-reduction advantages (Li et al., 2010; Wang et al., 2014).

In this study, we address these limitations by proposing a novel mechanical pretreatment method for LIBs using a zig-zag air separator targeting module-level crushing product. This innovative approach leverages differences in physical properties to achieve high recovery rates and efficient separation of LIB components. By optimizing particle size and airflow rates, the proposed method minimizes material losses and contamination risks while ensuring environmental sustainability. Unlike conventional methods, this approach provides a scalable and efficient solution for module-level recycling, bridging the gap between traditional practices and the growing need for advanced LIB recycling technologies. Through this work, we aim to establish a foundation for sustainable and economically viable LIB recycling practices that address the challenges of heterogeneity and complexity in spent batteries.

2. Samples and methods

2.1. Samples

Spent lithium-ion batteries (LIBs) were generously provided by a LIB recycling company located in Gunsan, South Korea. The battery modules were obtained through the disassembly of battery packs and were initially crushed using a 100 hp shredder at the recycling facility. The resulting crushed samples were subsequently dried to prepare them for the separation of foreign materials. Fig. 1 shows the battery module and the crushed battery module samples used in this study.

2.2. Experimental procedure on air separation

A laboratory zig-zag air separator, manufactured by HOSOKAWA ALPINE Aktiengesellschaft (Germany), was utilized for the separation tests (Fig. 2). The separation feasibility experiments were conducted on five primary materials (separator, cell pouch, electrodes, sponge, and plastic) recovered from the crushed battery module. To observe the separation behavior of each material and assess their separation characteristics, airflow was varied incrementally from 2.5 m^3/h to 35 m^3/h. Additionally, separation experiments were conducted using five different size fractions (6.7×4.75 mm, 4.75×3.35 mm, 3.35×1.7 mm, 1.7×0.85 mm, 0.85×0.425 mm) to examine the effect of particle size on separation efficiency.

(a)   (b)

Fig. 1. The (a) battery module and (b) crushed module sample used in this study

After examining the separation behavior of each individual material, mixed samples were prepared by combining materials according to the weight fractions found in the initial battery module. These mixed samples were separated under the same experimental conditions as the individual materials. This approach allowed for direct comparison of separation characteristics and aimed to evaluate the feasibility of applying air separation in practical processes.

All experiments utilized a sample weight of 10 g, and underflow and overflow samples were collected for each experimental condition. For each individual material, weight measurements were taken under various airflow conditions to determine the optimal airflow settings that maximize separation efficiency for each component. For the mixed samples, after measuring the weight of the underflow and overflow products, the components were manually separated by visual identification to evaluate the separation efficiency.

Fig. 2. Image of the zig-zag air separator utilized in the experimental setup, demonstrating the multi-stage structure for controlling particle trajectories and facilitating efficient separation

3. Theoretical consideration of air separation

The fundamental principle of the zig-zag air classifier revolves around the separation of particles based on their interaction with the airflow. This study utilizes the well-established drag force equation to quantitatively assess particle behavior in the air separator. The drag force is given by the equation (1) (Sadraey, 2009):

$$F_d = \frac{1}{2} C_d \rho v^2 A \tag{1}$$

where F_d represents the drag force experienced by a particle moving through a fluid, C_d is the drag coefficient, ρ is the air density, v is the relative velocity between particle and airflow, and A is the

projected area of the particle. It is assumed that particles will ascend when the drag force exceeds gravitational force, $F_g = mg$ (m: mass of sample, g: gravity constant) and conversely, they will descend when gravity is stronger than drag, forming the underflow product. Buoyancy also plays a role in particle movement, particularly for lighter particles, depending on air density and particle volume. Experiments were conducted over a range of airflow rates (2.5 m³/h to 35 m³/h) and particle size fractions (e.g., 6.7×4.75 mm, 4.75×3.35 mm, etc.). For accurate drag force calculation, the effective area and unit mass of each material were measured, and the average values were derived from the analysis of more than 50 samples. The effective area of the electrode was 0.69 cm², with a unit mass of 24 × 10³ g; the plastic had an effective area of 0.81 cm² and a unit mass of 110 ×10³ g; the pouch had an effective area of 0.74 cm² and a unit mass of 30 × 10³ g; and the separator had an effective area of 0.80 cm² and a unit mass of 2 × 10³ g. These values played a crucial role in validating the theoretical model by comparing them with the particle trajectories observed in the experiments.

4. Results

4.1. Composition of crushed battery module

To understand the characteristics of the crushed battery module (Fig. 1), both the particle size distribution and the mass ratio of different materials were analyzed. The analysis of the particle size distribution showed that particles larger than 19 mm accounted for 16.3% of the total mass. The remaining particle sizes were as follows: 19×9.5 mm (41.5%), 9.5×2 mm (28.7%), and below 2 mm (12.5%). Overall, particles larger than 10 mm accounted for approximately 58% of the total composition, indicating that the primary crushing of the battery module using the shredder was effective. Furthermore, the primary crushing process resulted in the detachment of some black mass powder from the electrodes, confirming that particles smaller than 2 mm made up 12.5% of the composition.

An examination of the components of the crushed battery module revealed not only typical materials such as electrodes, cell pouches, and separators from the battery cells, but also foreign materials including plastics, sponges, wires, and Fe-metal scraps (Fig. 3). After manually separating these components, the mass ratios were determined as follows: electrode/separator (81.13%), Fe-metal scrap (8.61%), plastic (4.73%), cell pouch (3.92%), sponge (1.00%), and wire (0.62%). This composition showed that approximately 85% of the materials were from the battery cell, while the remaining 15% consisted of foreign materials introduced during the battery module crushing process. Among these foreign materials, Fe-metal scraps must be removed as they can damage subsequent crushing processes and equipment. Additionally, organic materials such as plastic, sponge, and wire should also be removed, as they can negatively impact downstream processes, such as the leaching process. Fe-metal scrap can be effectively separated using magnetic separation, while wire can be removed by size separation due to its elongated shape.

(a) electrodes/separator	(b) plastic	(c) Fe-metal scrap
(d) sponge	(e) cell pouch	(f) wire
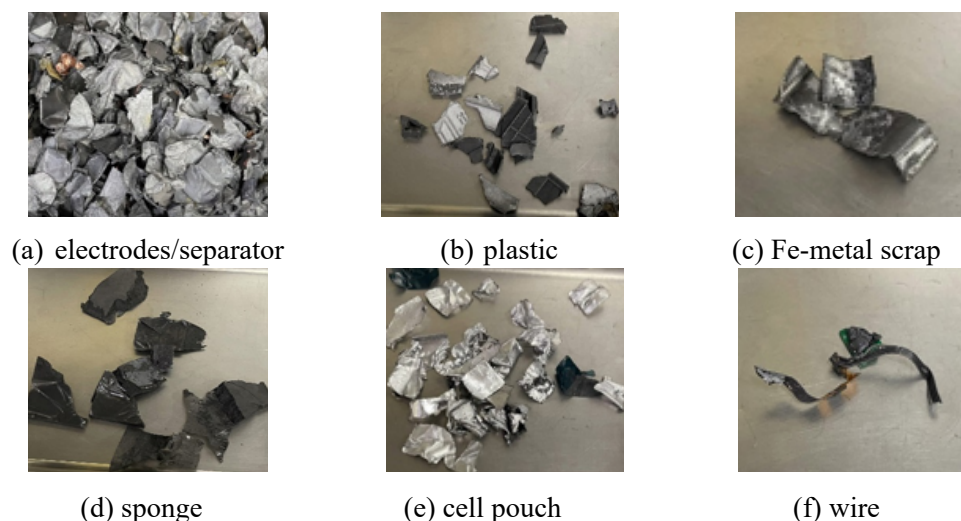
Fig. 3. Components of the crushed battery module. (a) electrodes/separator, (b) plastic, (c) Fe-metal scrap, (d) sponge, (e) cell pouch, and (f) wire. These materials were manually separated after crushing the battery module

Therefore, further experiments were planned to develop an effective method for separating the remaining four components, excluding Fe-metal scrap and wires. Considering the characteristics of these materials, an air classification method was chosen. Various experiments were conducted to determine effective separation conditions. To use a laboratory zig-zag air classifier, it was necessary to reduce the particle size of the crushed battery module due to input size limitations. The particle size distribution of each component produced by the cutting mill is shown in Table 1. These fractions were analyzed to evaluate their behavior during the air classification experiments and to determine the optimal separation conditions. For the three materials excluding the electrodes, particles in 1–5 mm range accounted for over 90% of total. For the electrodes, it was noted that during the cutting mill crushing process, the black mass became detach from the electrodes, resulting in a significant amount of fine particles smaller than 0.425 mm (31.48%). Samples from each particle size fraction were then used to evaluate their behavior in air classification.

Table 1. Particle size distribution of the main components crushed by a cutting mill

Size fraction (mm)	Plastic (%)	Cell pouch (%)	Electrodes (%)	Sponge (%)
6.70 × 4.75	0.31	0.92	0.98	2.30
4.75 × 3.35	8.62	24.78	2.14	30.17
3.35 × 1.70	62.35	52.60	15.27	45.02
1.70 × 0.85	20.23	11.80	34.89	11.79
0.85 × 0.425	5.81	2.71	15.25	4.90
< 0.425	2.69	7.20	31.48	5.82

4.2. Separating behavior of individual materials by air classifier

Fig. 4 illustrates the separation behaviors of individual materials using the zig-zag air separator. The air separator revealed distinct differences in separation behavior based on material type, particle size, and airflow rate. For example, the separation behavior of sponge, which has a relatively low density (0.1–0.5 g/cm³), differed significantly from other materials. Particles larger than approximately 1 mm were separated as overflow products even at a low airflow rate of 10 m³/h. However, as particle size decreased, a higher airflow rate was required to recover sponge as an overflow product (Fig. 4(a)). This is likely due to the significant influence of vortex flow within the zig-zag air separator, which affects smaller particles more than larger ones.

Electrodes and cell pouches exhibited similar trends in air classification (Fig. 4 (b), (c)). Sample recovery as overflow products began at lower airflow rates with decreasing particle size, but the overall trend remained consistent regardless of particle size, except for the smallest size fraction (0.85×0.425 mm) of the cell pouch. At an airflow rate of 10 m³/h, less than 10% of the sample was recovered as an overflow product, while over 90% was recovered at 20 m³/h. This behavior is attributed to the thin film-like shape of electrodes and cell pouches, which makes them more affected by particle shape than size during zig-zag air classification. During the electrode separation experiments, it was observed that the separator, initially combined with the electrodes, detached and exhibited independent behavior. Further experiments under identical conditions (Fig. 4(d)) showed that the separator was consistently separated as an overflow product at an airflow rate of 7.5 m³/h, regardless of particle size. This indicates that separator separation is more influenced by airflow rate rather than particle size. Plastic exhibited the greatest variability in separation behavior compared to other materials (Fig. 4(e)). Unlike the other materials, the plastic's separation trends varied significantly with particle size. For particle size fractions larger than 1.7 mm, almost the entire sample was distributed as an underflow product at airflow rates up to 20 m³/h, while all particles were separated as overflow products at 35 m³/h. However, as particle size decreased, the airflow rate required for recovery as overflow also decreased, with 25 m³/h needed for the 1.7×0.85 mm size fraction and only 15 m³/h for the 0.85×0.425 mm fraction. This indicates that plastic is more sensitive to airflow rate and particle size variations than other materials.

From the air classification experiments on various components of the crushed battery module across different particle sizes, it was determined that the sponge and separator could be selectively separated as an overflow product at an airflow rate of 10 m³/h. For the electrodes and cell pouches, selective separation as an overflow product was feasible at airflow rates of 20–25 m³/h. However, plastics

exhibited significant variation in separation behavior depending on particle size, indicating the need for precise particle control to achieve effective separation.
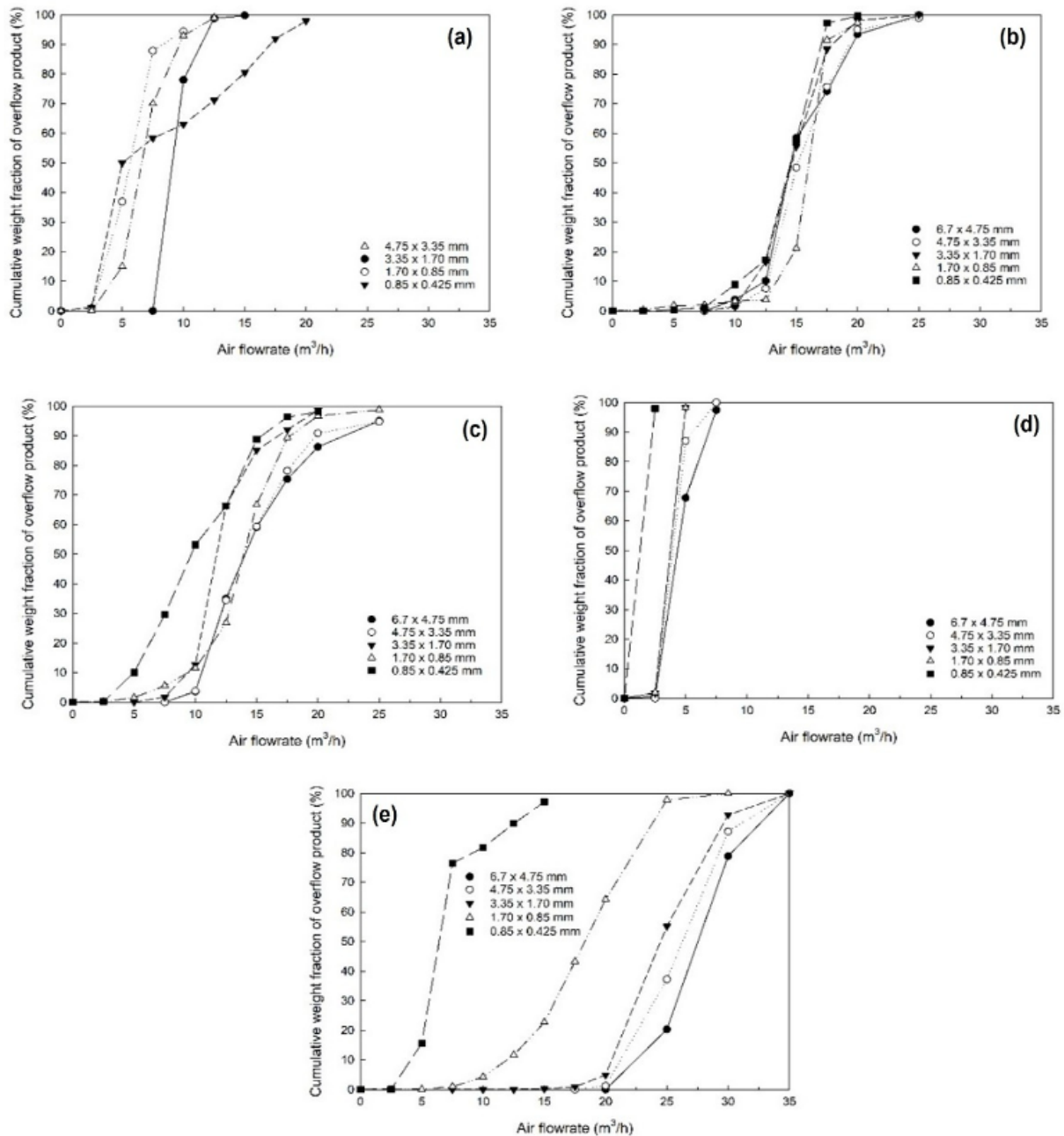
Fig. 4. Cumulative weight fraction of the overflow product of individual materials at various size fractions. The Fig. shows the separation behavior of (a) sponge, (b) electrodes, (c) cell pouch, (d) separator, and (e) plastic using the zig-zag air separator

4.3. Theoretical behavior of individual materials by air classifier

This section builds upon the analysis in Section 4.2, which explored the behavior of individual materials, focusing on theoretical predictions, specifically the effective drag coefficients, and their influence on the separation behavior of materials in the zig-zag air classifier. The experimental results are compared with these theoretical predictions to validate the proposed model.

The effective drag coefficients for various materials in the zig-zag air separator are shown in Fig. 5. Fig. 5 illustrates the separation behavior of lighter materials, such as separators, which achieve floating at lower airflow rates, and heavy materials, like plastics, which require higher airflow velocities for effective separation. The data highlights the relationship between material density, drag force, and the

airflow thresholds necessary for floating and separation. It shows that lighter materials, such as separators, remain floating at lower airflow velocities, while heavy materials, like plastics, require higher airflow velocities for effective separation. These findings further validate the theoretical model and emphasize the importance of adjusting airflow to separate materials with varying densities. Lighter materials, such as separators, were found to be easily floating at lower airflow velocities due to their higher surface area-to-mass ratios. These materials exhibit lower drag coefficients, making them more sensitive to airflow. On the other hand, heavy materials, such as plastics, require higher airflow velocities for effective separation because of their greater mass and higher drag coefficients.

Experimental observations confirmed that the theoretical model accurately predicted the separation behavior of materials. Lighter materials were more easily separated as overflow products, while less heavy materials required higher airflow rates for floating. For example, separators were efficiently separated at lower airflow rates (around 5 m³/h), while plastics required higher velocities (above 20 m3/h) for efficient separation. These results emphasize the importance of controlling airflow to achieve optimal separation based on the physical properties of the materials. At a theoretical effective drag coefficient (C_d = 0.19), the separation points for plastic, electrodes/pouch, and separators were 25.1 m³/h, 15.0 m³/h, and 4.7 m³/h, respectively, which closely matched the actual experimental results. This confirmed that the calculated effective drag coefficient is appropriate for predicting separation efficiency in the zig-zag classifier. These results further validate the theoretical model and underscore the importance of adjusting airflow based on the physical properties of each material. In particular, effective separation of materials with varying densities requires precise adjustments to airflow velocity.
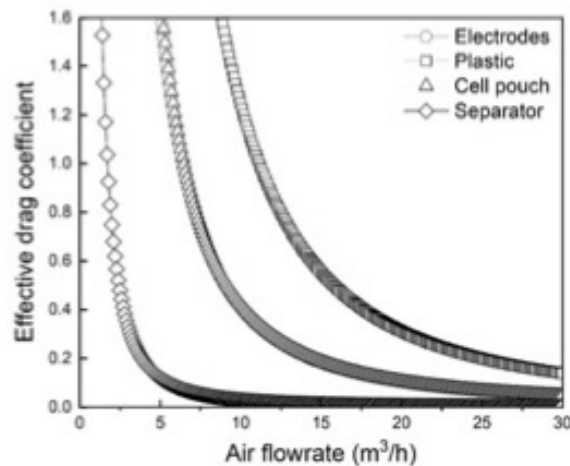
Fig. 5. Effective drag coefficients for various materials in the zig-zag air separator as a function of airflow rate

4.4. Separating behavior of mixed materials by air classifier

Experimental data for each material, categorized by particle size, is presented in Fig. 6. These tests aimed to verify the separation potential of each component through air classification across various particle sizes. Sponge test results were excluded due to their minimal proportion in the overall composition compared to other materials. The experimental conditions, based on Fig. 4, were optimized to ensure accurate and effective separation across all materials. As shown in Fig. 4, the airflow rates for the separator were set to 10 m³/h, and 20 m³/h for electrodes and cell pouches, in line with previous studies. These conditions were adjusted as particle size decreased, leading to optimized recovery. Fig. 6 shows the cumulative weight fraction of the overflow product as a function of size fractions. These results illustrate how material separation efficiency varies with particle size and airflow rate. Table 2 presents the mass fractions of separator, cell pouch, electrodes, and plastic for different size fractions and airflow rates. These results illustrate the separation efficiency for each component under different conditions of particle size and airflow rate. For the separator, 100% recovery was achieved at a 5 m³/h airflow rate for the smallest particle size fraction (0.85×0.425 mm). As particle size increased, the required airflow rate for effective separation also increased. At 7.5 m³/h, overflow separation of the separator was achieved across all particle sizes, with a 99.6% recovery and 0.4% loss. For electrodes and cell pouches, effective recovery was observed within the 10–20 m³/h airflow range, as confirmed by the experiments

conducted at different particle sizes. The recovery for electrodes was 95.7%, with a 4.3% loss, and for cell pouches, it was 95.6%, with a 4.4% loss. For plastics, effective separation occurred for particles larger than 3.35 mm at 20 m³/h underflow, yielding a recovery rate of over 97%. However, smaller particles (less than 1.7 mm) exhibited a sharp drop in recovery to 78.7%, indicating that smaller particle sizes hinder effective separation. The overall recovery for plastics was 91.9%, with an 8.1% loss. These findings demonstrate the high efficiency of the zig-zag air separation method in LIB recycling, with consistently high recovery rates for separator, electrodes, cell pouch, and plastic across various particle sizes. Even for components with lower recovery rates, such as plastic, the method still yields substantial material recovery.
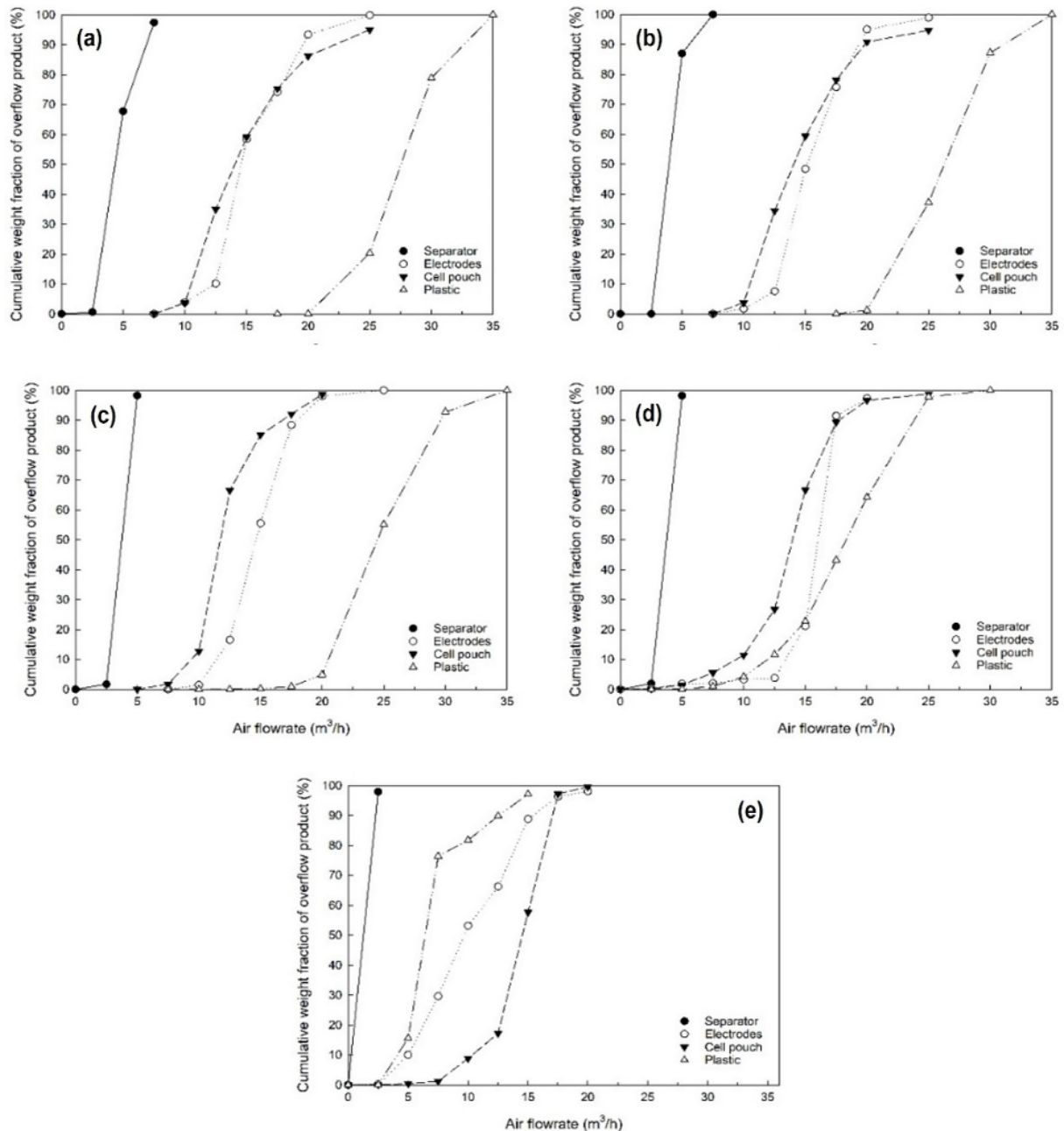
Fig. 6. Cumulative weight fraction of the overflow product as a function of size fractions. The Fig. shows the separation behavior of mixed materials using the zig-zag air separator across various particle size fractions: (a) 6.7×4.75 mm, (b) 4.75×3.35 mm, (c) 3.35×1.70 mm, (d) 1.70×0.85 mm, and (e) 0.85×0.425 mm

The process flow for battery module crushing and pre-treatment is outlined in Fig. 7. This flowsheet incorporates module crushing followed by air classification techniques to effectively separate and recover desired materials from crushed battery modules. The process highlights the stages for efficient

material recovery, emphasizing the importance of pre-treatment methods for optimizing LIB recycling. This flowchart illustrates the steps involved in separating and recovering materials from crushed battery modules. The diagram shows the use of zig-zag air separation at 7.5 m³/h and 20 m³/h airflow rates, followed by a second crushing step, ensuring high recovery rates for all components. In addition, Fig. 7 provides a visual representation of the recovery process, highlighting how the separator, electrodes, cell pouch, and plastic are separated at each stage. The Fig. clearly demonstrates the optimized airflow rates and separation behavior, showcasing the efficiency of the proposed method for LIB recycling. This optimized process flow, combined with the material recovery data, underscores the effectiveness of the zigzag air separation technique in ensuring high recovery rates and minimal contamination.

Table 2. Mass fractions (%) of separated components from mixed samples at various conditions

Size fraction	Air flowrate	Separator	Cell pouch	Electrodes	Plastic
6.70 × 4.75	5 m³/h OF*	87.23	-	-	-
	7.5 m³/h OF	11.56	-	0.64	-
	10 m³/h OF	1.20	3.83	0.28	-
	20 m³/h OF	-	91.15	94.80	0.35
	20 m³/h UF**	-	5.02	4.28	99.65
4.75 × 3.35	5 m³/h OF	97.56	-	-	-
	7.5 m³/h OF	2.44	-	0.64	-
	10 m³/h OF	-	10.34	0.90	-
	20 m³/h OF	-	85.04	94.15	2.69
	20 m³/h UF	-	4.62	4.31	97.31
3.35 × 1.70	5 m³/h OF	100	-	-	-
	7.5 m³/h OF	-	-	0.63	-
	10 m³/h OF	-	15.62	4.21	-
	20 m³/h OF	-	81.25	92.58	21.28
	20 m³/h UF	-	3.13	2.58	78.72

* OF : overflow, ** UF : underflow
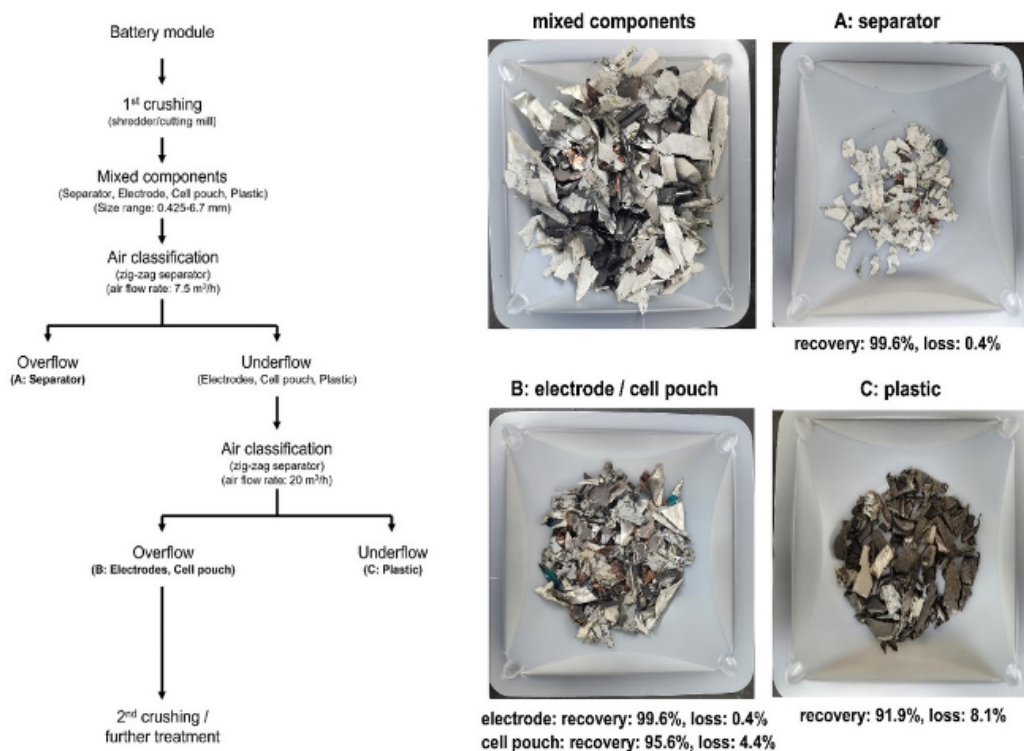
Fig. 7. Process flow for battery module crushing and pre-treatment. The flowchart illustrates the steps for separating and recovering materials from crushed battery modules using zig-zag air separation. The Fig. demonstrates the separation of key components: (a) separators, (b) electrodes/cell pouches, and (c) plastics

5. Discussions

In this study, we introduced a novel approach for the recycling of spent lithium-ion batteries (LIBs) using a zig-zag air separator targeting module-level crushing product. Our results show significant improvements in recovery rates when compared to existing methods in the literature. Specifically, our method achieved recovery rates of 99.6% for separators, 95.7% for electrodes, 95.6% for cell pouches, and 91.9% for plastics at 1.7×6.7 mm size fraction, demonstrating a high level of efficiency across multiple material components.

Existing studies, such as those by Heelan et al. (2016) and Wagner-Wenz et al. (2023), have employed mechanical methods combined with flotation or air classification techniques for the recycling of LIBs. Heelan et al. (2016) reported recovery rates in the range of 80–90% for electrodes and separators, while Wagner-Wenz et al. (2023) achieved recovery rates of 85–90% for certain components. While these methods have contributed significantly to the field, they still require several energy-intensive steps and may involve additional processes like flotation or chemical treatments to achieve optimal separation. Our approach, which combines crushing and air classification in a single step, offers a more streamlined and energy-efficient solution. The results from our zig-zag air separator show not only a higher recovery rate but also a reduction in contamination between fractions, leading to cleaner and more useful components for further processing. For example, our method achieved 99.6% recovery for separators, which is notably higher than those reported in other methods, particularly for plastics, where our recovery rate of 91.9% surpasses the 70–80% typically reported in the literature.

While our study did not examine the subsequent recycling stages, the high recovery rates and low material loss suggest that the separated components, separators, electrodes, cell pouches, and plastics, could be efficiently utilized in downstream processes like hydrometallurgy or pyrometallurgy. These fractions, with their high purity, can serve as valuable input for further refining and reuse.

We believe that the zig-zag air separation method offers significant advantages over traditional methods, particularly in terms of process simplicity, energy efficiency, and separation effectiveness. This method holds considerable promise for large-scale industrial applications due to its ability to separate multiple materials with minimal contamination. Future work will focus on further optimizing the process parameters, such as airflow rates and particle size distributions, to enhance the method's efficiency across a wider range of LIB types. Additionally, investigating direct recycling pathways for the recovered components will provide insights into the potential for full-scale industrial implementation.

6. Conclusions

This study introduces a novel mechanical pretreatment method for the efficient recycling of lithium-ion batteries (LIBs) by combining module-scale crushing with zig-zag air separation. The optimized process achieves high recovery rates for key components, such as separators, electrodes, cell pouches, and plastics, by carefully adjusting particle size and airflow rates. Specifically, recovery rates of 97% were achieved for plastics larger than 3.35 mm, while electrodes and cell pouches demonstrated recovery rates of 95% at airflow rates between 7.5 and 20 m³/h. These results emphasize the importance of precise particle size control and airflow optimization to maximize separation efficiency and reduce contamination.

The integration of air separation with mechanical crushing significantly improves overall recycling efficiency, streamlining the process and reducing the need for complex downstream treatments. This approach not only conserves valuable materials but also minimizes environmental impact, making it a sustainable alternative to conventional recycling methods. The findings suggest that this method is highly adaptable to large-scale industrial applications, providing a cost-effective and scalable solution for early stage of LIB mechanical recycling process.

Future research should focus on integrating this early stage of mechanical pretreatment with hydrometallurgical or pyrometallurgical processes to further enhance material recovery. Additionally, exploring the applicability of this method to different types and configurations of LIBs will be crucial in optimizing recycling efficiency across diverse battery chemistries. By addressing these areas, this technique has the potential to play a pivotal role in establishing a circular economy for LIBs, contributing to sustainable resource management and reduced environmental footprint.

Acknowledgement

Reference

CHANGES, A., POSPIECH, B., 2013. *A brief review on hydrometallurgical technologies for recycling spent lithium-ion batteries*. Journal of Chemical Technology & Biotechnology, 88, 1191–1199.

CHEN, M., MA, X., CHEN, B., ARSENAULT, R., KARLSON, P., SIMON, N., WANG, Y., 2019. *Recycling end-of-life electric vehicle lithium-ion batteries*. Joule, 3, 2622–2646.

DUNN, J.B., GAINES, L., SULLIVAN, J., WANG, M., 2012. *Impact of recycling on cradle-to-gate energy consumption and greenhouse gas emissions of automotive lithium-ion batteries*. Environmental Science & Technology, 46, 12704–12710.

FAN, E., LI, L., WANG, Z., LIN, J., HUANG, Y., YAO, Y., CHEN, R., WU, F., 2020. Sustainable recycling technology for Li-ion batteries and beyond: challenges and future prospects, 120, 7020–7063.

GAINES, L., 2014. *The future of automotive lithium-ion battery recycling: charting a sustainable course*. Sustainable Materials and Technologies. 1–2, 2–7.

GEORGI-MASCHLER, T., FRIEDRICH, B., WEYHE, R., HEEGN, H., RUTZ, M., 2012. *Development of a recycling process for Li-ion batteries*. Journal of Power Sources, 207, 173–182.

GRATZ, E., SA, E., APELIAN, D., WANG, Y., 2014. *A closed loop process for recycling spent lithium ion batteries*, Journal of Power Sources, 262, 255–262.

HE, B., ZHENG, H., TANG, K., XI, P., LI, M., WEI, L., GUAN, Q., 2024. *A comprehensive review of lithium-ion battery (LiB) recycling technologies and industrial market trend insights*, Recycling, 9, 9.

HEELAN, J., GRATZ, E., ZHENG, Z., WANG, Q., CHEN, M., APELIAN, D., WANG, Y., 2016. *Current and prospective Li-ion battery recycling and recovery processes*. JOM, 68, 2632–2638.

LI, L., Ge, J., WU, F., CHEN, R., CHEN, S., WU, B., 2010. *Recovery of cobalt and lithium from spent lithium ion batteries using organic citric acid as leachant*. Journal of Hazardous Materials, 176, 288–293.

MAKUZA, B., TIAN, Q., GUO, X., CHATTOPADHYAY, K., YU, D., 2021. *Pyrometallurgical options for recycling spent lithium-ion batteries: a comprehensive review*, Journal of Power Sources, 491, 229622.

PINEGAR, H., SMITH, Y.R., 2019. *End-of-life lithium-ion battery component mechanical liberation and separation. JOM.* 71, 4447–4456.

RENIER, O., PELLINI, A., SPOOREN, J., 2023. *Advances in separation of graphite from lithium iron phosphate from end-of-life batteries shredded fine fraction using simple froth flotation*. Batteries, 9, 589.

VELAZQUEZ-MARTINEZ, O., VALIO, J., SANTASALO-AARNIO, A., REUTER, M., SERNA-GUERRERO, R., 2019. *A critical review of lithium-ion battery recycling processes from a circular economy perspective*, Batteries, 5, 68.

WAGNER-WENZ, R., ZUILICHEN, A.-J., Göllner-Völker, L., Berberich, K., Weidenkaff, A., & Schebek, L. 2023. *Recycling routes of lithium-ion batteries: A critical review of the development status, the process performance, and life-cycle environmental impacts*. MRS Energy & Sustainability, 10, 1–34.

WANG, X., GAUSTAD, G., BABBITT, C.W., RICHA, K., 2014. *Economic of scale for future lithium-ion battery recycling infrastructure*. Resources, Conservation and Recycling, 83, 53–62.

XU, J., THOMAS, H.R., FRANCIS, R.W., LUM, K.R., WANG, J., LIANG, B., 2008. *A review of processes and technologies for the recycling of lithium-ion secondary batteries*. Journal of Power Sources, 177, 512–527.

YAN, S.-X., JIANG, Y.-Z., CHEN, X.-P., YUAN, L., MIN, T.-T., CAO, Y., PENG, W.-L., ZHOU, T., 2023. *Engineering classification recycling of spent lithium-ion batteries through pretreatment: a comprehensive review from laboratory to scale-up application*. Rare Metals, 43, 915–941.

ZHANG, X., Li, L., FAN, E., XUE, Q., BIAN, Y., WU, F., CHEN, R., 2018. *Toward sustainable and systematic recycling of spent rechargeable batteries*, Chemical Society Reviews, 47, 7239–7302.